Supplement of Atmos. Meas. Tech., 8, 5063–5087, 2015
http://www.atmos-meas-tech.net/8/5063/2015/
doi:10.5194/amt-8-5063-2015-supplement

Atmospheric Measurement Techniques
Open Access

Supplement of

ACTRIS ACSM intercomparison – Part 1: Reproducibility of concentration and fragment results from 13 individual Quadrupole Aerosol Chemical Speciation Monitors (Q-ACSM) and consistency with co-located instruments

V. Crenn et al.

Correspondence to: J. Sciare (j.sciare@cyi.ac.cy)

Supplement S1. Ambient air measurements

Table S1.

Average values (±1σ) of Q-ACSM diagnostic parameters (Airbeam, chamber temperature, inlet pressure and vaporizer temperature).

Q-ACSM #	Airbeam (10^{-7})	Chamber temperature (°C)	Inlet Pressure (Torr)	Vaporizer temperature (°C)
#1	1.35 ± 0.020	37 ± 1.5	1.33 ± 0.02	601.0 ± 8.3
#2	0.95 ± 0.033	33 ± 0.4	1.33 ± 0.01	603.5 ± 0.49
#3	0.95 ± 0.049	40 ± 3.1	1.25 ± 0.02	595.3 ± 3.1
#4	0.90 ± 0.054	33 ± 0.5	1.23 ± 0.01	601.7 ± 0.40
#5	0.97 ± 0.025	35 ± 0.7	1.49 ± 0.01	586.5 ± 3.1
#6	0.80 ± 0.115	33 ± 0.4	1.20 ± 0.01	607.9 ± 7.8
#7	1.03 ± 0.043	36 ± 1.1	1.40 ± 0.01	600.9 ± 2.42
#8	0.89 ± 0.068	31 ± 0.5	1.33 ± 0.01	594.0 ± 3.4
#9	0.94 ± 0.032	37 ± 0.7	1.21 ± 0.10	596.6 ± 0.24
#10	1.04 ± 0.024	35 ± 0.4	1.22 ± 0.01	596.6 ± 0.27
#11	0.96 ± 0.085	36 ± 0.6	1.23 ± 0.01	599.8 ± 0.21
#12	0.92 ± 0.042	30 ± 0.6	1.31 ± 0.01	603.4 ± 0.22
#13	0.93 ± 0.168	31 ± 0.4	1.32 ± 0.01	590.8 ± 1.6

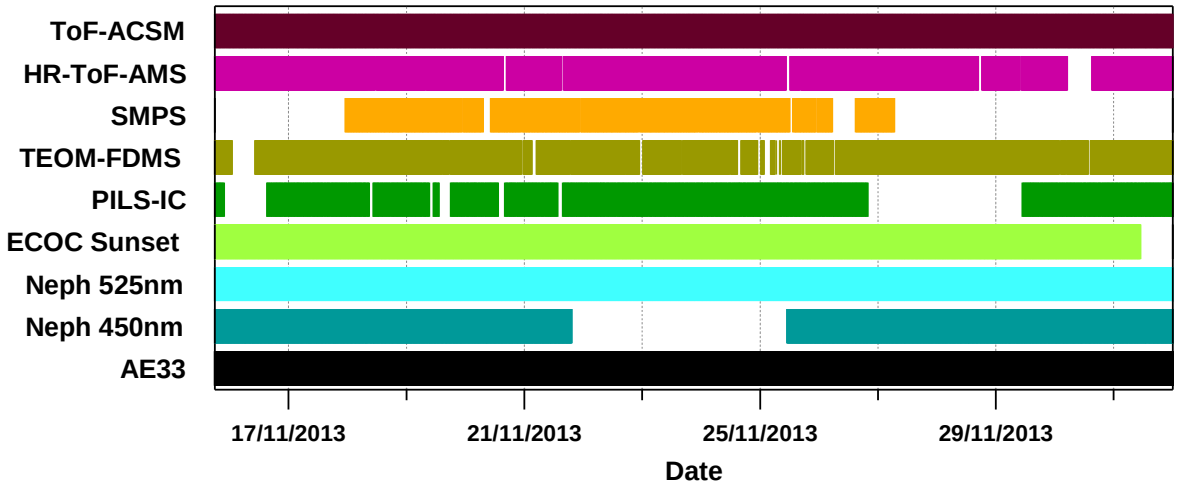

Figure S1. Temporal coverage of co-located instruments deployed during the intercomparison study.

Supplement S2. Effects of the use of individual Q-ACSM sulfate relative ion efficiencies

Use of sulfate relative ion efficiency values obtained from the first calibration phase

It is recalled here that RF_{NO3}, RIE_{NH4} and RIE_{SO4} values obtained from calibrations performed at the beginning of the study were discarded, and that only RF_{NO3} and RIE_{NH4} could be estimated from calibrations performed at the end of campaign. A default RIE_{SO4} value of 1.2 ($RIE_{SO4,def}$) was then applied to calculate sulfate mass concentrations. The reasons of this choice are given in Sect. 3.1.2. Here, we present the effect of Q-ACSM-independent RIE_{SO4} (RIE_{SO4} values measured at the beginning of the intercomparison exercise for each Q-ACSM, noted RIE_{SO4}^{*} thereafter) to calculate the SO_4 mass concentrations. The RIE_{SO4}^{*}, $RIE_{SO4,def}$ values and $RIE_{SO4,def}$-to-RIE_{SO4}^{*} ratios are given in Table B1, respectively. $RIE_{SO4,def}$-to-RIE_{SO4}^{*} ratios varied by a factor of 2 ranging from 1.24 (Q-ACSM #5) to 2.50 (Q-ACSM #2).

The temporal variability of the median mass concentrations and range (minimum, maximum) of SO_4 measured by the 13 Q-ACSMs and linear correlation plots for SO_4 mass concentrations obtained with RIE_{SO4}^{*} values are shown in Fig. B1, and Fig. B2, respectively. Slopes varied from 0.58 (Q-ACSM #7) to 1.88 (Q-ACSM #2) while they only varied from 0.62 (Q-ACSM #10) to 1.47 (Q-ACSM #5) with a constant value of 1.2, highlighting a higher dispersion of SO_4 measurements using individual Q-ACSM RIE_{SO4} values.

Table S2.1.

Average RIE_{NH4} and RIE_{SO4} values determined from Q-ACSM calibrations

Q-ACSM #	$\mathbf{RIE_{NH4,meas}}$	$\mathbf{RIE_{SO4,def}}$	$\mathbf{RIE_{SO4}^{*}}$	$\mathbf{RIE_{SO4,def} / RIE_{SO4}^{*}}$
#1	3.37	1.2	0.82	1.46
#2	14.72	1.2	0.48	2.50
#3	5.48	1.2	0.71	1.69
#4	8.98	1.2	0.70	1.71
#5	3.42	1.2	0.97	1.24
#6	4.72	1.2	0.70	1.71
#7	7.24	1.2	0.87	1.38
#8	6.45	1.2	0.62	1.94
#9	3.56	1.2	0.76	1.58
#10	7.79	1.2	0.56	2.14
#11	3.17	1.2	0.67	1.79
#12	3.83	1.2	0.71	1.69
#13	9.36	1.2	0.87	1.38

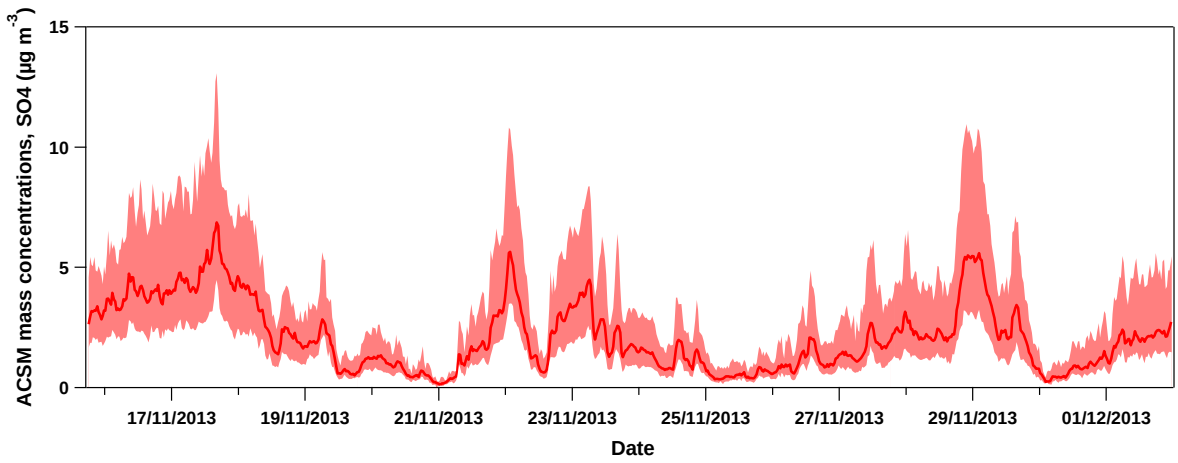

Figure S2.1. Averaged sulfate mass concentrations measured by the 13 Q-ACSMs using an instrument-dependent RIE_{SO4}^{*}. Dark red line and color area correspond to the median of Q-ACSMs and the min-max range, respectively.

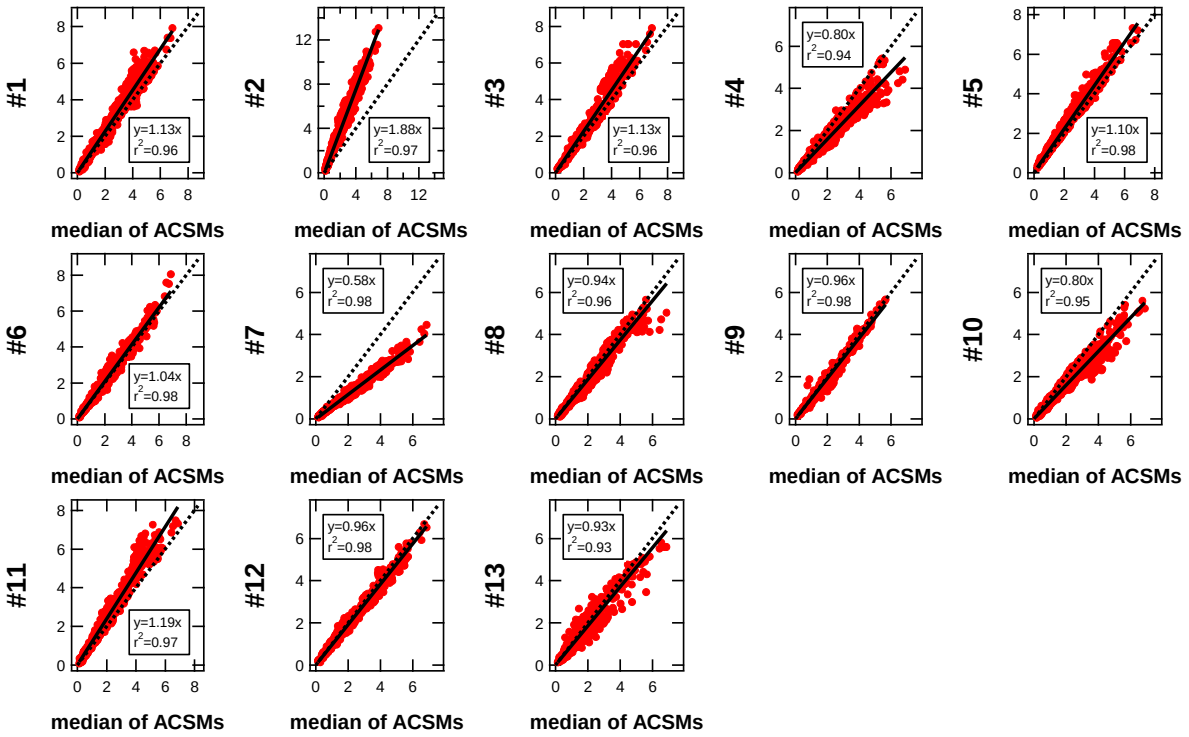

Figure S2.2. Scatter plots of sulfate mass concentrations in µg m^{-3} measured by each Q-ACSM versus the median of all the 13 Q-ACSMs, for which an instrument-dependent RIE_{SO4}^{*} was applied. Dotted line is the 1:1 line. Full lines represent the orthogonal distance regression fits with zero intercept.

Use of sulfate relative ionization efficiency values calculated assuming full neutralization of secondary inorganic aerosols

For each instrument, the RIE_{SO4} value needed to obtain full neutralization of secondary inorganic aerosols ($RIE_{SO4,neut}$) could be estimated by fitting Q-ACSM measured and predicted SO_4 values ($SO_{4,meas}$ and $SO_{4,pred}$, respectively), where $SO_{4,pred}$ is the estimated value of SO_4 and calculated as follows:

$$SO_{4,pred} = \frac{NH_{4,meas} - \left(\frac{MW(NH_4)}{MW(NO_3)}\right) NO_{3,meas} - \left(\frac{MW(NH_4)}{MW(Cl)}\right) Cl_{meas}}{2\left(\frac{MW(NH_4)}{MW(SO_4)}\right)} \quad (B1)$$

where MW(s) is the Molecular Weight of the chemical species (s), $SO_{4,meas}$, $NO_{3,meas}$, Cl_{meas}, and $NH_{4,meas}$ are the SO_4, NO_3, Cl, and NH_4 mass concentrations measured by the Q-ACSMs, respectively.

$RIE_{SO4,neut}$ is then estimated dividing the RIE default value ($RIE_{SO4,def}$ = 1.2) by the slope of $SO_{4,pred}$ vs. $SO_{4,meas}$. $RIE_{NH4,meas}$, $RIE_{SO4,def}$, $RIE_{SO4,neut}$ and $RIE_{SO4,def}$-to-$RIE_{SO4,neut}$ values used/calculated for each Q-ACSM are given in Table B2. $RIE_{SO4,def}$-to-$RIE_{SO4,neut}$ ratios varied significantly from 0.13 (Q-ACSM #2) to 4.81 (Q-ACSM #9). Although RIE_{SO4} measured values above the default value of 1.2 have been recently reported in the literature for a few calibrations conducted by participants (Petit et al., 2015; Ripoll et al., 2015) those values were quite close to the default 1.2 value (i.e., 1.25 and 1.26, respectively). By contrast, very low/high $RIE_{SO4,neut}$ obtained here for some instruments does not make sense and can only be discarded.

The temporal variability of the median mass concentrations and range (minimum, maximum) of SO_4 measured by the 13 Q-ACSMs and linear correlation plots for SO_4 mass concentrations obtained with $RIE_{SO4,neut}$ values are shown in Fig. B3, and Fig. B4, respectively. Slopes varied from 0.13 (Q-ACSM #4) to 2.44 (Q-ACSM #9) while they only varied from 0.62 (Q-ACSM #10) to 1.47 (Q-ACSM #5) with a constant value of 1.2, again highlighting a higher dispersion of SO_4 measurements using individual Q-ACSM RIE_{SO4} values. It should be noted that the methodology described in the present subsection to estimate RIE_{SO4} (*a posteriori* and using ambient data) could be attempted here due to previous data showing full neutralization of both sulfate and nitrate by ammonium in the Paris area and during this period of the year (e.g. Bressi et al., 2013). Nevertheless, we do not mean that the use of such a methodology should be promoted for RIE_{SO4} calculation within future studies.

Table S2.2.

Average RIE values calculated assuming ion full neutralization of ambient aerosols

Q-ACSM #	**$RIE_{NH4,meas}$**	**$RIE_{SO4,def}$**	**$RIE_{SO4,neut}$**	**$RIE_{SO4,def}$ / $RIE_{SO4,\ neut}$**
#1	3.37	1.2	0.61	1.96
#2	14.72	1.2	9.40	0.13
#3	5.48	1.2	0.84	1.43
#4	8.98	1.2	8.30	0.14
#5	3.42	1.2	0.59	2.04
#6	4.72	1.2	0.54	2.22
#7	7.24	1.2	2.32	0.52
#8	6.45	1.2	0.47	2.54
#9	3.56	1.2	0.25	4.81
#10	7.79	1.2	3.36	0.36
#11	3.17	1.2	0.36	3.37
#12	3.83	1.2	0.48	2.48
#13	9.36	1.2	5.43	0.22

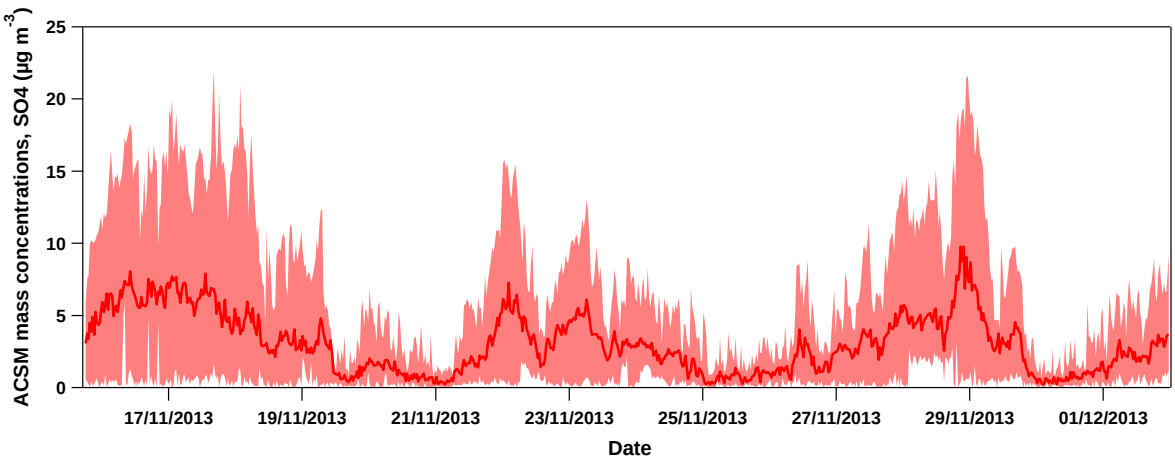

Figure S2.3. Averaged sulfate mass concentrations predicted for the 13 Q-ACSMs using an instrument-dependent $RIE_{SO4,neut}$. Dark red line and color area correspond to the median of Q-ACSMs and the min-max range, respectively.

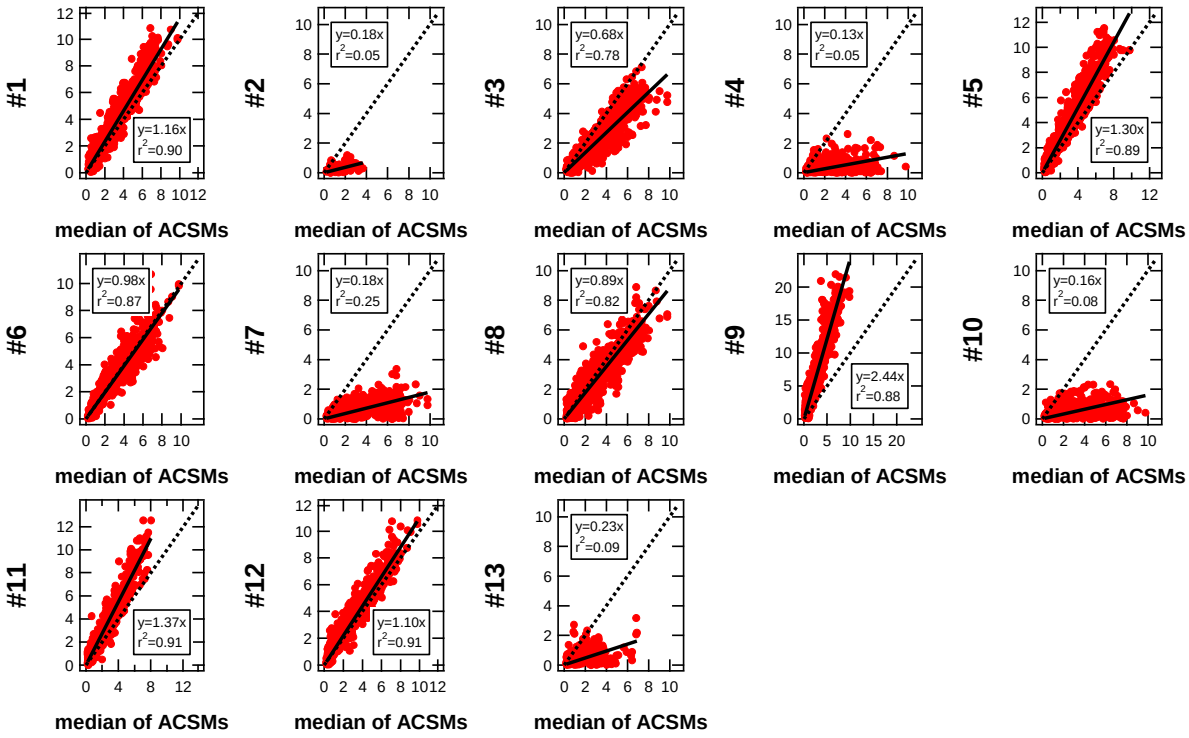

Figure S2.4. Scatter plots of sulfate mass concentrations in µg m^{-3} predicted for each Q-ACSM versus the median of all the 13 Q-ACSMs, for which an instrument-dependent $RIE_{SO4,neut}$ was applied. The median of all the 13 Q-ACSMs was calculated as the median value of the $SO_{4,pred}$ concentrations of each Q-ACSM. Many data points were discarded here, due to high uncertainties associated with low NH_4 mass concentrations that may led to negative $SO_{4,pred}$ values calculated from Eq. (B1). Some negative $SO_{4,pred}$ were also obtained for periods with high concentrations of NH_4NO_3 and resulted from high uncertainties associated by the difference of two elevated and close concentrations (e.g. [NH_4] - [NH_4] from NH_4NO_3). This is particularly true for Q-ACSM #2 and 13, and to a lesser extent for Q-ACSM #4, 7 and 10. Dotted line is the 1:1 line. Full lines represent the orthogonal distance regression fits with zero intercept.

Supplement S3. Q-ACSM data correction

Collection efficiency (CE)

The calculation of mass concentrations is depending on a collection efficiency (CE) for both Q-ACSMs and HR-ToF-AMS measurements. The CE correction is accounting for (i) particle bouncing at the inverted-conical vaporizer inducing an incomplete detection of aerosol species (Matthew et al., 2008) (ii) particle losses in the aerodynamic lenses (iii) broadening of the particle beam (Huffman et al., 2005), and (iv) several factors such as high aerosol acidity, ammonium nitrate mass fraction (ANMF) and organic liquid contents and/or relative humidity (Middlebrook et al., 2012). The ANMF is calculated as follows:

$$\mathrm{ANMF} = \frac{(80/62)\mathrm{NO_3}}{(\mathrm{NH_4} + \mathrm{SO_4} + \mathrm{NO_3} + \mathrm{Cl} + \mathrm{OM})} \quad \text{(C1)}$$

where NH_4, SO_4, NO_3, Cl, and OM are the measured aerosol ammonium, sulfate, nitrate, chloride, and organic mass concentrations (in $\mu g\ m^{-3}$).

In the present study, a composition-dependent CE (CE_{ANMF}) was calculated from the following Eqs. (C2) and (C3), adapted from Middlebrook et al. (2012) parameterizations:

$$\mathrm{CE_{ANMF}} = 0.0833 + 0.9167 \times \mathrm{ANMF} \quad \text{(C2)}$$

$$\mathrm{CE} = \max(0.5, \mathrm{CE_{ANMF}}) \quad \text{(C3)}$$

The temporal variability of the CE we have used during our study is presented in the Fig. C1, below.

For ACSMs (and also AMS), the particle acidity has commonly been estimated based on the ion balance between nitrate, sulfate (and possibly chloride) and ammonium measurements. Due to issues related to RIE_{NH4} and RIE_{SO4} calibrations, highlighted in the present study, such calculations should then be performed and interpreted circumspectly. Moreover, Hennigan et al. (2015) have recently shown that the ion balance or molar ratios of cations and anions may not be a good proxy for aerosol pH, reinforcing the need to handle such calculations with caution.

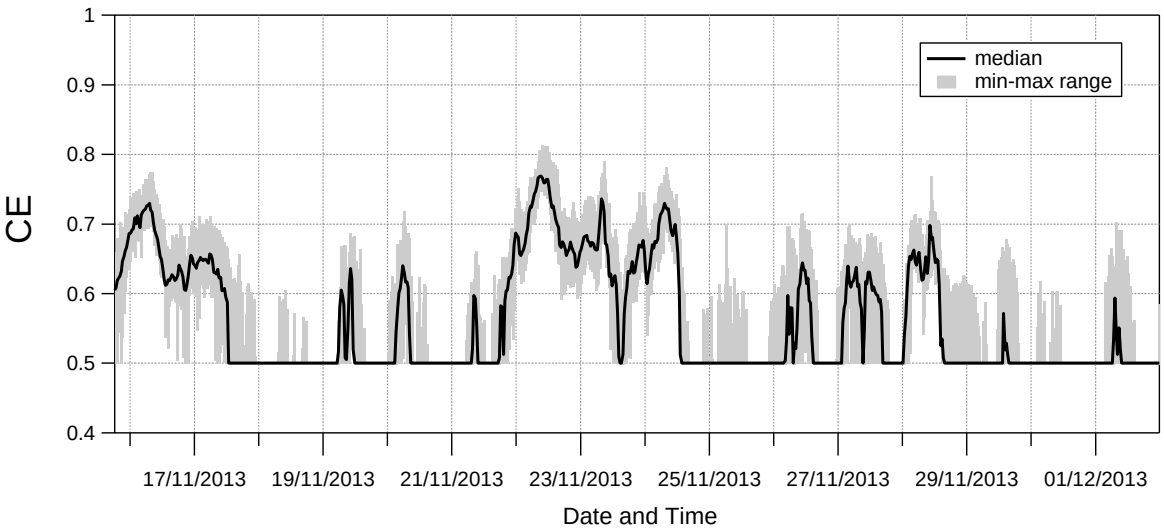

Figure S3. Time series of Q-ACSM collection efficiency (CE) applied to the 13 Q-ACSMs adapting the procedure given in Middlebrook et al. (2012). The median and the min-max range of the 13 Q-ACSMs are presented in dark black lines and light grey area, respectively.

Supplement S4. Z-score analysis parameters

Table S4.

Statistical analysis values used within Z-score calculations for NR-PM_1 mass concentrations and their major components (OM, NO_3, SO_4, NH_4, and Cl), expressed in µg m^{-3}, obtained from the data of the 13 Q-ACSMs (N = 780). Raw data values are given for information, while robust approach values are those actually used in the present study.

	Raw data[a]			Robust approach[b]				
	Mean value	Standard deviation (σ)	Variation coefficient (%)	Robust mean (x*)	Robust standard deviation (s*)	Recalculated standard deviation (σ_p)[c]	Standard deviation of the assigned value (µ*)	Relative confidence interval (%)
NR-PM_1	15.7	2.58	16.5	16.9	1.56	1.68	0.616	20.9
OM	6.57	1.19	18.1	6.55	1.22	1.29	0.423	40.6
NO_3	5.29	0.892	16.9	5.20	0.770	0.823	0.290	33.0
SO_4	1.28	0.334	26.0	1.27	0.358	0.378	0.124	61.2
NH_4	2.38	0.973	40.9	2.28	0.817	0.873	0.308	79.6
Cl	0.136	0.160	117	0.186	0.102	0.109	0.039	122

[a] formula of raw data parameters are given in ISO 5725-2

[b] formula of robust approach parameters are available in ISO 5725-5 and ISO 13528

[c] calculated from the quadratic sum of s* and µ* because the number of Q-ACSMs is below 16.

Supplement S5. Q-ACSM standard diagnostic ion plots for each Q-ACSM and additional statistical Z-score results

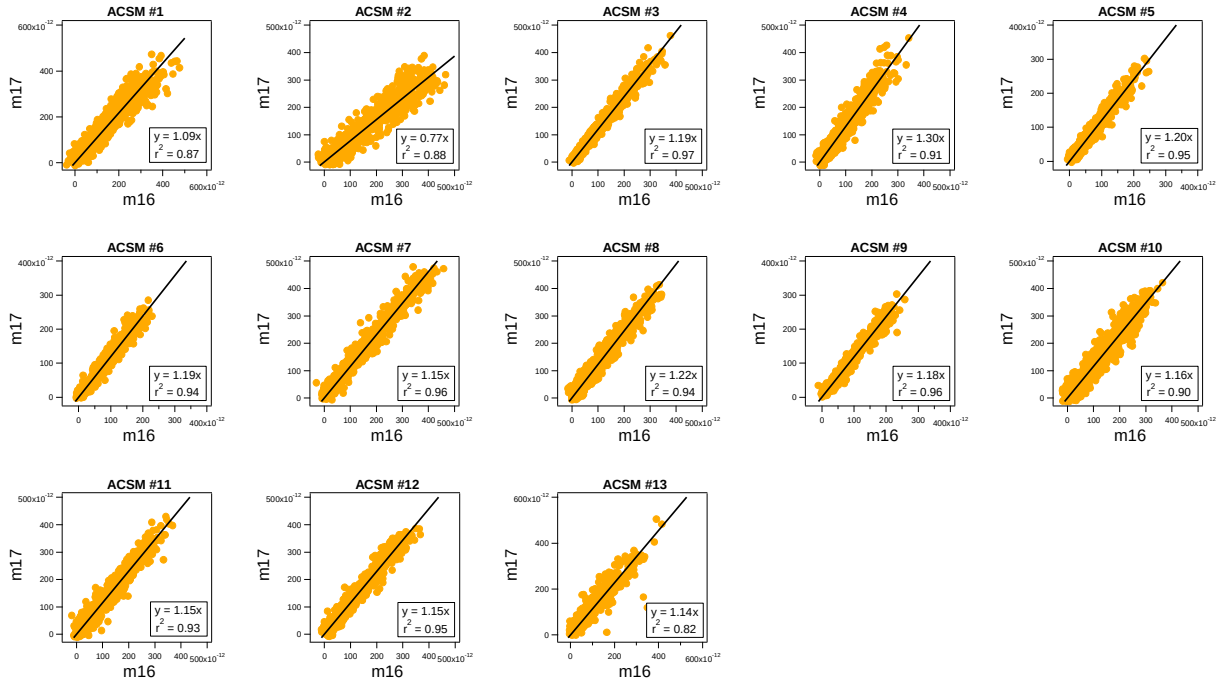

Figure S5.1. Standard diagnostic ion plots of Q-ACSM NH_4 m17 vs. m16. Orthogonal linear regression fits were plotted with zero intercept.

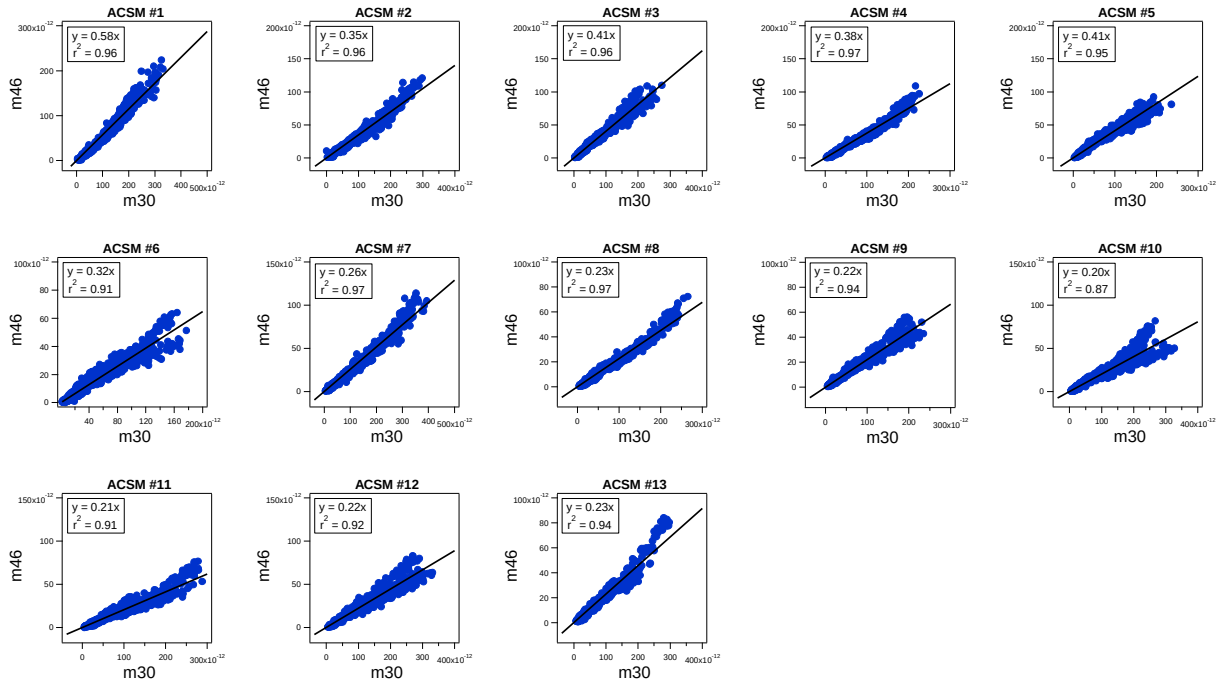

Figure S5.2. Standard diagnostic ion plots of Q-ACSM NO_3 m46 vs. m30. Orthogonal linear regression fits were plotted with zero intercept.

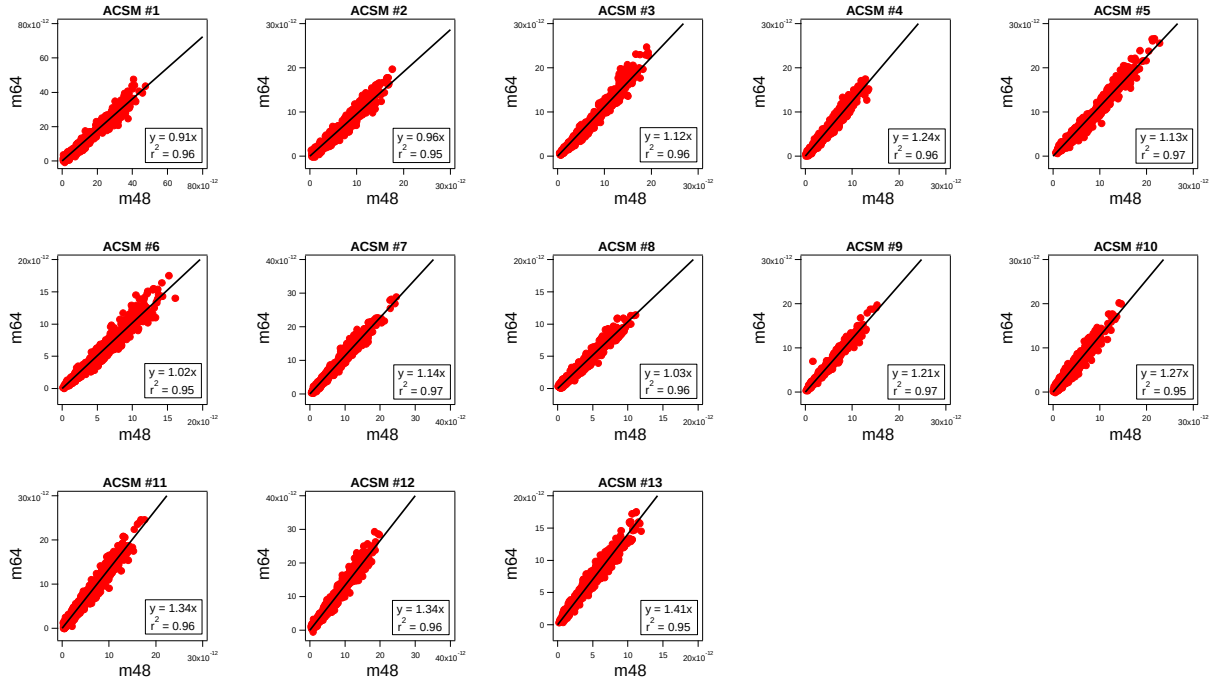

Figure S5.3. Standard diagnostic ion plots of Q-ACSM SO_4 m64 vs. m48. Orthogonal linear regression fits were plotted with zero intercept.

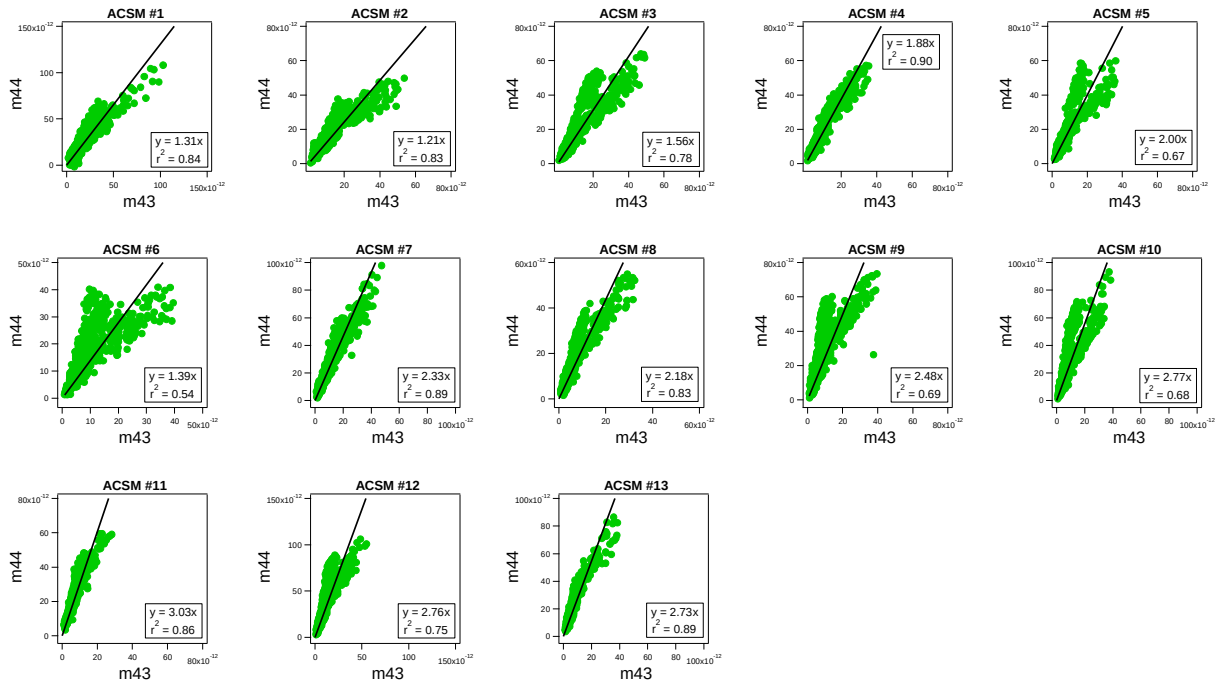

Figure S5.4. Standard diagnostic ion plots of Q-ACSM Org m44 vs. m43. Orthogonal linear regression fits were plotted with zero intercept.

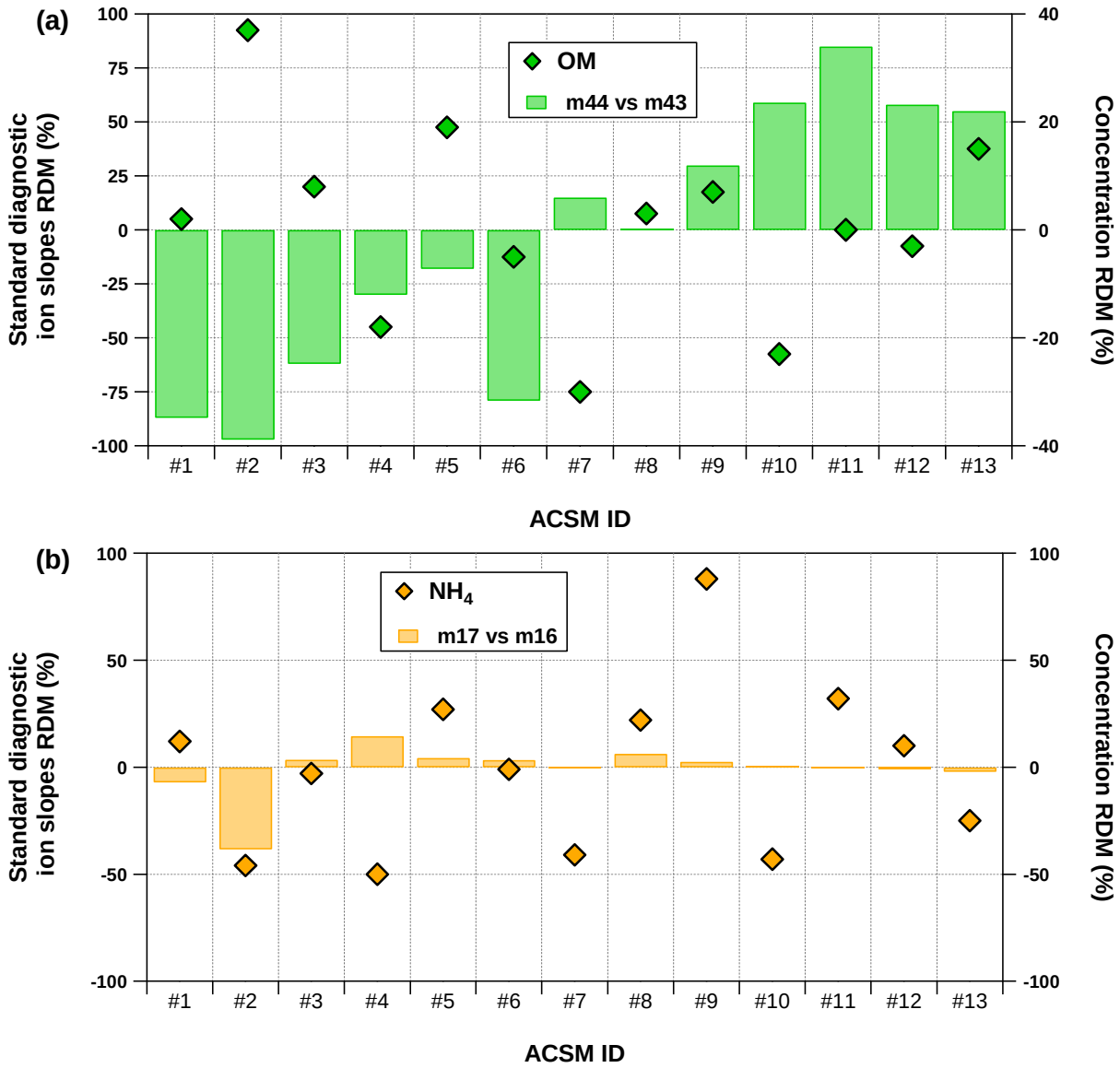

Figure S5.5. Relative deviations to the median (RDM) of Q-ACSM concentrations and standard diagnostic ion slopes for (a) OM (m44 vs. m43), (b) NH_4 (m17 vs. m16), (c) NO_3 (m46 vs. m30), and (d) SO_4 (m64 vs. m48, m80 vs. m48, m81 vs. m48 and m98 vs. m48) obtained from orthogonal distance regression fits with zero intercept.

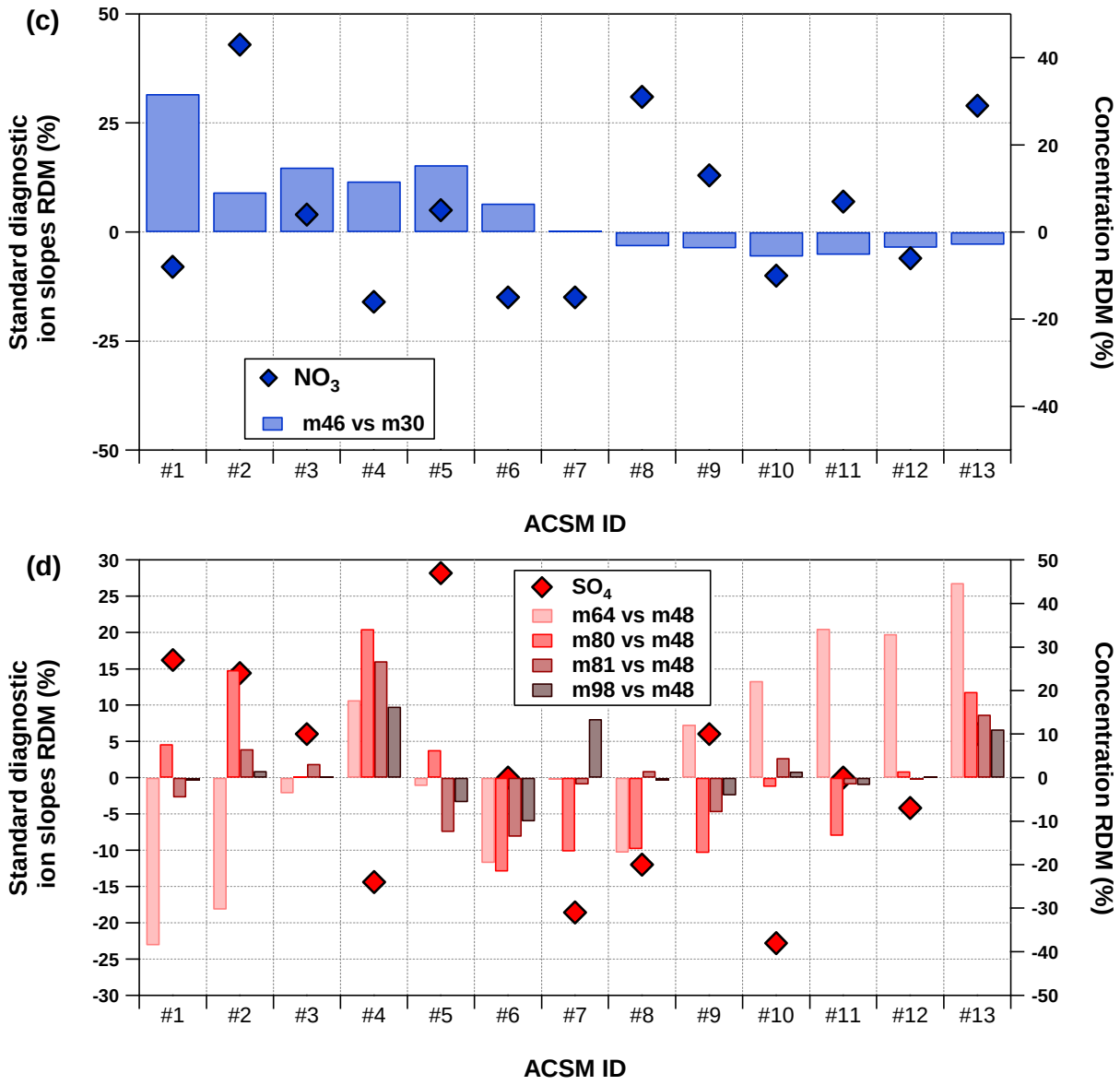

Figure S5.5. continued.

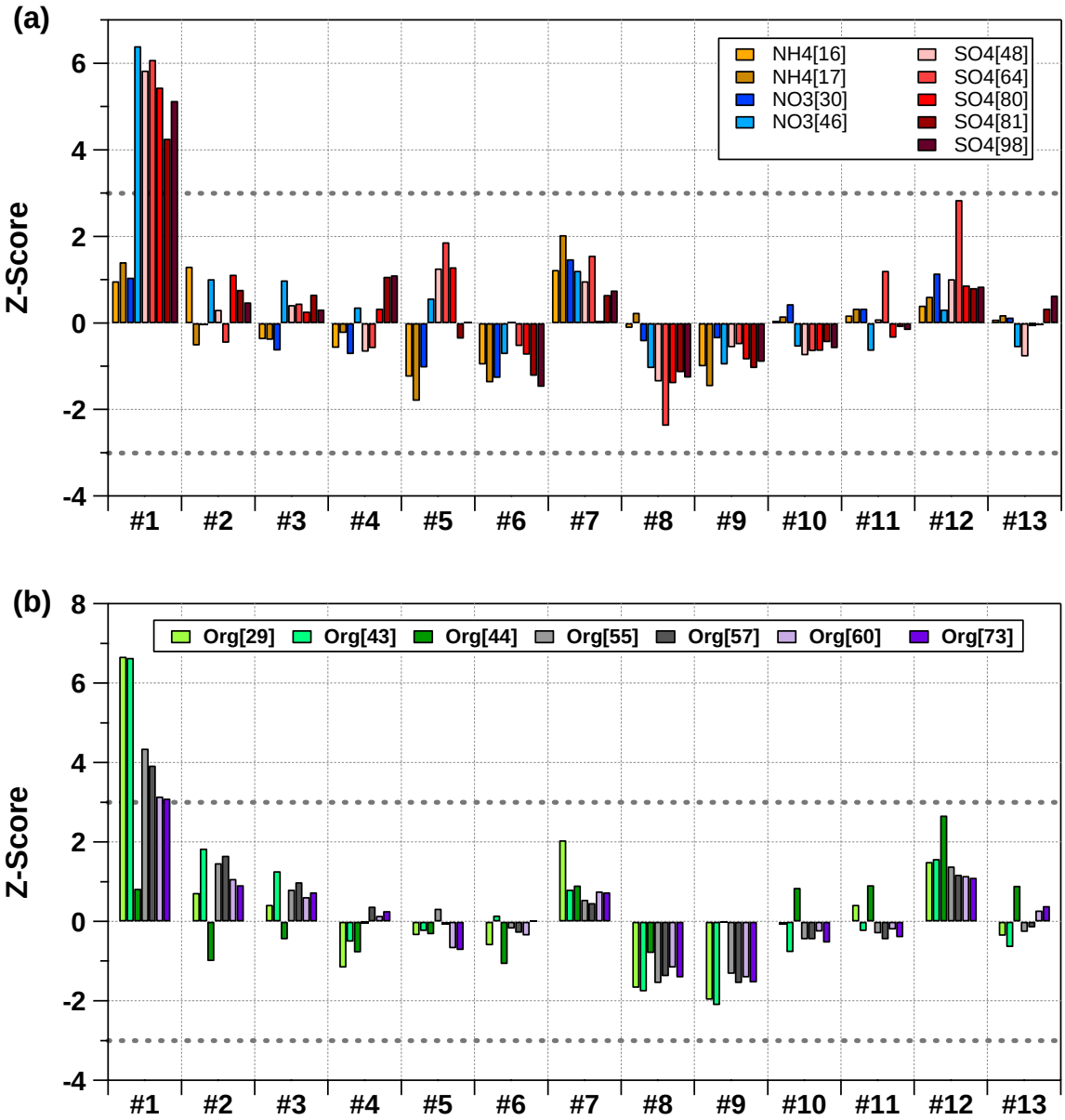

Figure S5.6. Statistical Z-score results for major Q-ACSM fragments associated to (a) inorganics (*m/z* 16 and 17 for ammonium, *m/z* 30 and 46 for nitrate, and *m/z* 48, 64, 80, 81, and 98 for sulfate) and (b) organic matter (*m/z* 29, 43, 44, 55, 57, 60, and 73).

Supplement S6. Chemical and optical mass closures

Influence of a time-dependent density on SMPS PM_1 mass concentrations and comparability with Q-ACSM PM_1.

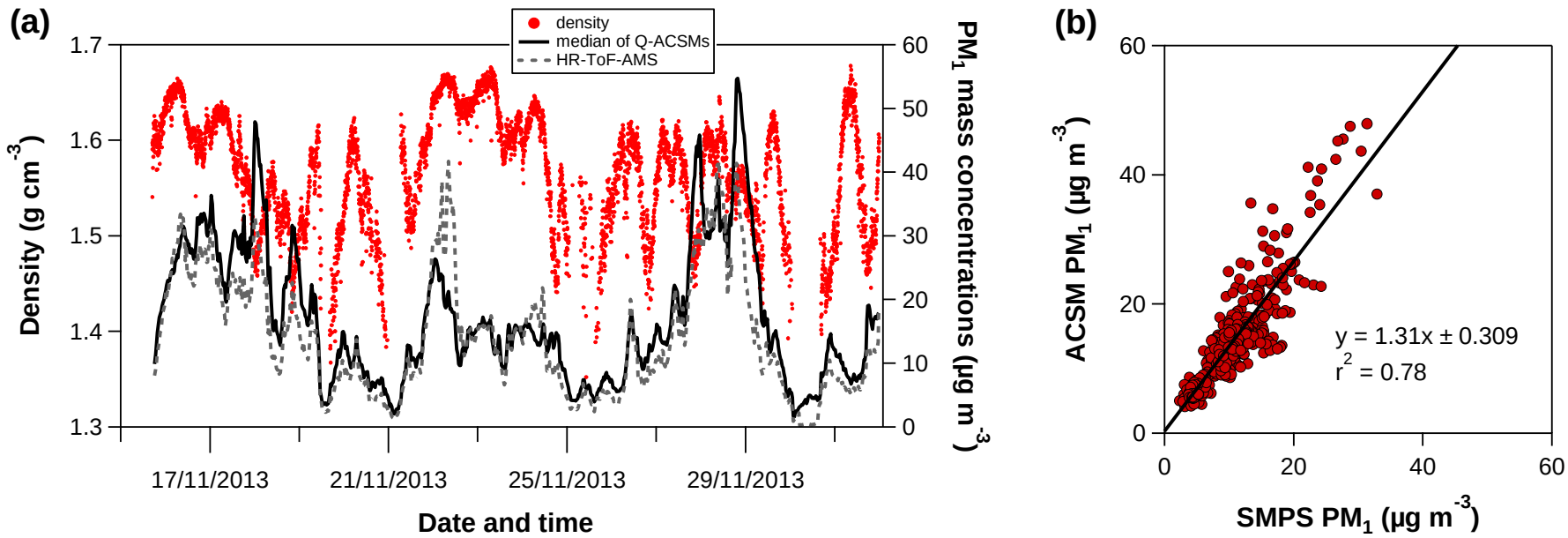

Figure S6.1. (a) Time series of the time-dependent density (red circle dots) and PM_1 mass concentrations in µg m^{-3} measured by the HR-ToF-AMS (dotted grey line) and the median of the 13 Q-ACSMs (solid black line) and (b) scatter plots of PM_1 mass concentrations measured by the median of the 13 Q-ACSMs vs. SMPS PM_1 mass concentrations calculated using a time-dependent density.

Scatter plots between ACSM and co-located online instruments

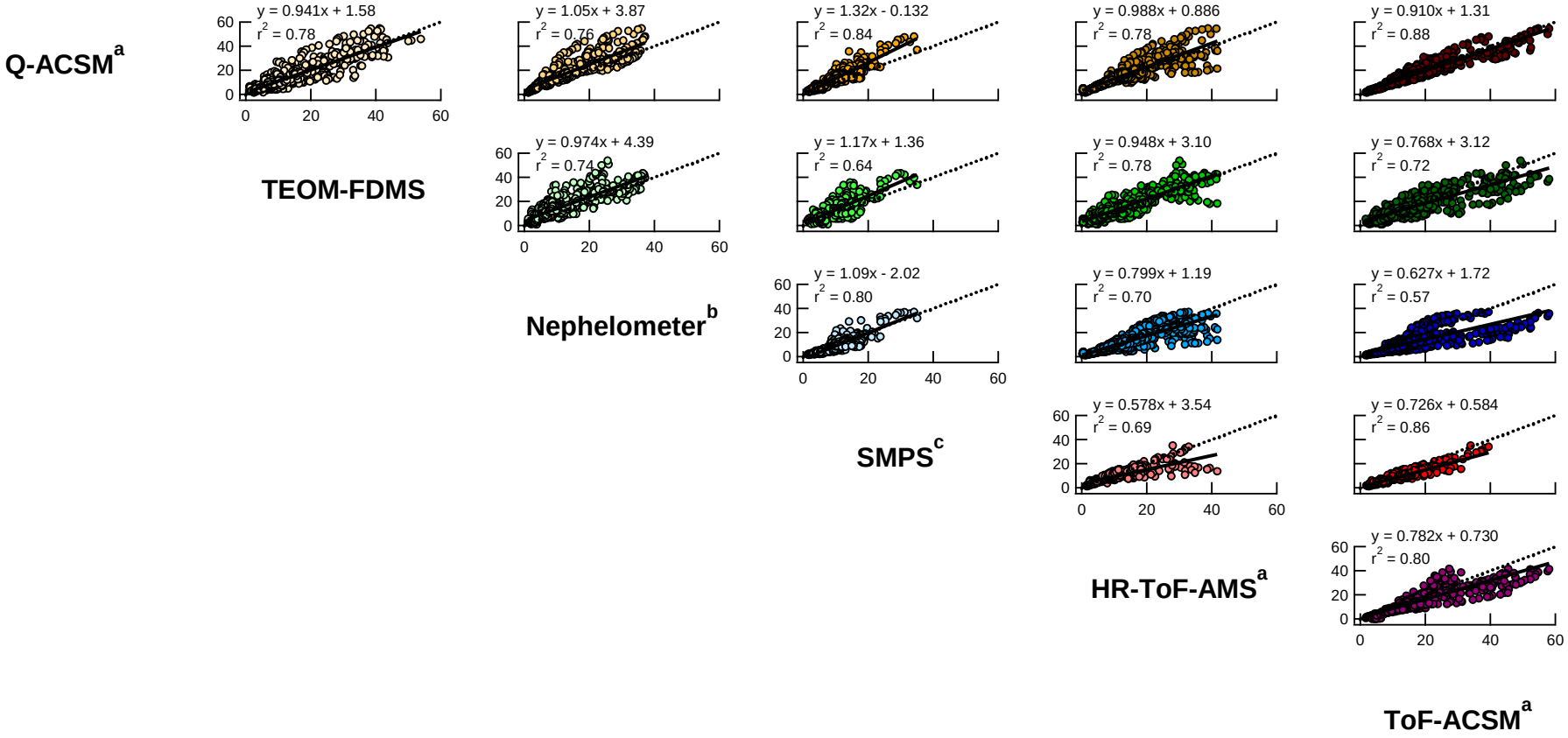

[a]: PM_1 mass was determined from the sum of all non-refractory components (OM, NO_3, SO_4, NH_4, and Cl) and EBC mass concentrations. Moreover, Q-ACSM, ToF-ACSM, and HR-ToF-AMS mass concentrations were corrected assuming a time-dependent CE according to the procedure described by Middlebrook et al. (2012); [b]: A mass scattering efficiency of 2.5 $m^2\ g^{-1}$ was used to reconstruct PM_1 mass (Titos et al., 2012); [c]: PM_1 mass was calculated using an averaged aerosol density of 1.6 based on the NR-PM_1 mass composition measured by HR-ToF-AMS.

Figure S6.2. PM_1 correlation plots between instruments deployed during the intercomparison study. All the concentrations in µg m^{-3} were 3-h averaged (N = 780). Black solid and dotted lines represent the orthogonal distance regression with non-zero intercept fits and 1:1 lines, respectively.

Optical mass closure

The reconstruction of the light scattering coefficient was performed following the same methodology as given in Sciare et al. (2008). Briefly, a simple model assuming an external mixing of the particles with constant dry mass scattering efficiencies and constant aerosol types can be used here to reconstruct the light scattering coefficient (σ_{sp}), as follows:

$$\sigma_{sp} = \alpha_{ions} f(RH)([(NH_4)_2SO_4] + [NH_4NO_3]) + \alpha_{POM}[POM] + \alpha_{sea\ salt}[sea\ salt] + \alpha_{dust}[dust] \quad \text{(F1)}$$

where α_s represents the mass scattering efficiency of the chemical species (s). It is assumed here that $(NH_4)_2SO_4$ and NH_4NO_3 have a mass scattering efficiency of 3 $m^2\ g^{-1}$ while particulate organic matter and sea salt have mass scattering of 3.9 and 4.3 $m^2\ g^{-1}$, respectively. The light scattering contribution of dust was neglected here due to both their low concentrations and mass scattering efficiencies. A constant enhancement factor, f(RH), was taken as equal to 1 after checking that the nephelometer measurements (λ = 525 nm) were not significantly affected by water uptake onto aerosols. The RH was kept below 40% during the whole study. The light scattering measured by the latter instrument was then compared to the reconstructed light scattering (Fig. F3). A good agreement was observed (r^2 = 0.83; slope = 0.93). The difference may be due to propagation uncertainties associated with the measurements of the different species by the different techniques (i.e., nephelometer, OCEC Sunset analyser, Q-ACSM) and the estimation of the mass scattering coefficients biases the reconstructed light scattering values.

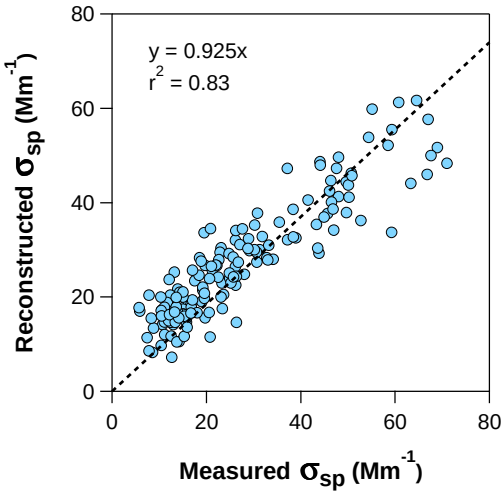

Figure S6.3. Optical mass closure calculated between the reconstructed versus measured σ_{sp}.

References

Hennigan, C. J., Izumi, J., Sullivan, A. P., Weber, R. J., and Nenes, A.: A critical evaluation of proxy methods used to estimate the acidity of atmospheric particles, Atmos. Chem. Phys., 15, 2775-2790, doi:10.5194/acp-15-2775-2015, 2015.

Huffman, J. A., Jayne, J. T., Drewnick, F., Aiken, A. C., Onasch, T., Worsnop, D. R., and Jimenez, J. L.: Design, modeling, optimization, and experimental tests of a particle beam width probe for the aerodyne aerosol mass spectrometer. Aerosol Sci. Tech., 39(12), 1143-1163, 2005.

ISO, 5725-2: Accuracy (trueness and precision) of measurement methods and results—Part 2: Basic method for the determination of repeatability and reproducibility of a standard measurement method. International Organization for Standardization: Geneva, 1994.

ISO, 5725-5: Accuracy (trueness and precision) of measurement methods and results-Part 5: Alternative methods for the determination of the precision of a standard measurement method. International Organization for Standardization, Geneva, 1998.

ISO, 13528: Statistical methods for use in proficiency testing by interlaboratory comparison. International Organization for Standardization, Geneva, 2005.

ISO/IEC, 17025: General requirements for the competence of testing and calibration laboratories. International Organization for Standardization, Geneva, 1999.

Matthew, B. M., Middlebrook, A. M., & Onasch, T. B.: Collection efficiencies in an Aerodyne Aerosol Mass Spectrometer as a function of particle phase for laboratory generated aerosols. Aerosol Sci. Tech., 42(11), 884-898, 2008.

Middlebrook, A. M., Bahreini, R., Jimenez, J. L. and Canagaratna, M. R.: Evaluation of Composition-Dependent Collection Efficiencies for the Aerodyne Aerosol Mass Spectrometer using Field Data, Aerosol Sci. Tech., 46(3), 258–271, doi:10.1080/02786826.2011.620041, 2012.

Petit, J.-E., Favez, O., Sciare, J., Crenn, V., Sarda-Estève, R., Bonnaire, N., Močnik, G., Dupont, J.-C., Haeffelin, M. and Leoz-Garziandia, E.: Two years of near real-time chemical composition of submicron aerosols in the region of Paris using an Aerosol Chemical Speciation Monitor (ACSM) and a multi-wavelength Aethalometer, Atmos. Chem. Phys., 15(6), 2985–3005, doi:10.5194/acp-15-2985-2015, 2015.

Ripoll, A., Minguillón, M. C., Pey, J., Jimenez, J. L., Day, D. A., Sosedova, Y., Canonaco, F., Prévôt, A. S. H., Querol, X., and Alastuey, A.: Long-term real-time chemical characterization of submicron aerosols at Montsec (southern Pyrenees, 1570 m a.s.l.), Atmos. Chem. Phys., 15, 2935-2951, doi:10.5194/acp-15-2935-2015, 2015.

Sciare, J., Sarda-Estève, R., Favez, O., Cachier, H., Aymoz, G. and Laj, P.: Nighttime residential wood burning evidenced from an indirect method for estimating real-time concentration of particulate organic matter (POM), Atmos. Environ., 42(9), 2158–2172, doi:10.1016/j.atmosenv.2007.11.053, 2008.

Titos, G., Foyo-Moreno, I., Lyamani, H., Querol, X., Alastuey, A., & Alados-Arboledas, L.: Optical properties and chemical composition of aerosol particles at an urban location: An estimation of the aerosol mass scattering and absorption efficiencies. J. Geophys. Res. Atmos., 117(D4), 1984–2012, 2012.